Hydrodynamic interaction of swimming organisms in an inertial regime

Gaojin Li,[1] Anca Ostace,[2] and Arezoo M. Ardekani[1,*]
[1]*School of Mechanical Engineering, Purdue University, West Lafayette, Indiana 47907, USA*
[2]*Aerospace and Mechanical Engineering, University of Notre Dame, Notre Dame, Indiana 46556, USA*
(Received 7 June 2016; published 4 November 2016)

We numerically investigate the hydrodynamic interaction of swimming organisms at small to intermediate Reynolds number regimes, i.e., Re $\sim$ O(0.1–100), where inertial effects are important. The hydrodynamic interaction of swimming organisms in this regime is significantly different from the Stokes regime for microorganisms, as well as the high Reynolds number flows for fish and birds, which involves strong flow separation and detached vortex structures. Using an archetypal swimmer model, called a "squirmer," we find that the inertial effects change the contact time and dispersion dynamics of a pair of pusher swimmers, and trigger hydrodynamic attraction for two pullers. These results are potentially important in investigating predator-prey interactions, sexual reproduction, and the encounter rate of marine organisms such as copepods, ctenophora, and larvae.

DOI: 10.1103/PhysRevE.94.053104

I. INTRODUCTION

Collective dynamics in microorganism suspensions, bird flocks, and fish schools has received much attention in the past few years. These flows share many similarities despite the Reynolds number $\mathrm{Re} = \rho U a/\mu$ ranging across several orders of magnitudes. Here, U and a are the speed and length scale of the organism, and ρ and μ are the density and dynamic viscosity of the surrounding fluid. The Reynolds numbers of typical swimmers are Re $\sim 10^{-5}$ for bacteria, 10^{-3} for *Chlamydomonas*, 0.01–0.1 for *Volvox* [1], 0.2 for *Paramecia* in the swimming mode and 2 in the escaping mode [2], 100 for *Pleurobrachia*, and 20–150 for copepods [3]. Within the low Reynolds number regime (Re $= 10^{-5}$–10^{-3}), bacteria in dense suspensions show a collective motion, including large-scale flow structures and vortices [4], locally correlated motions [5], spatial inhomogeneities of the swimmer distribution, and enhanced diffusion and mixing [6]. Similar phenomena were also observed in the collective motions of microtubules [7], spermatozoa [8], self-motile colloidal particles [9], and vibrating granular systems [10]. At higher Reynolds numbers (Re $> 10^3$), schooling fish, flocking birds and swarming insects use collective motion to their advantage to reduce predation risk and to increase the success rate of feeding and reproduction [11]. At the base of each of these phenomena is the hydrodynamic interaction between the moving bodies and their detached vortical structures that leads to higher swimming (or flying) efficiency [12,13].

The hydrodynamic interaction between microorganisms is important to the dynamics of the suspension of swimmers. In a dilute suspension, the leading-order effect of a freely swimming organism in a Stokes regime behaves as a force dipole [14], whose induced velocity field decays as $1/r^2$. Based on the sign of the force dipole, microswimmers can be distinguished as pushers, which push the fluid away from the front and the back of their bodies, such as bacteria and spermatozoa, and pullers, which do the opposite, such as algae. The swimmer directly affects other cells by the induced velocity field and reorients their swimming direction by the induced velocity gradients. The trajectories of two interacting microswimmers are strongly affected by the swimming mechanism, the relative displacement, and orientation of the swimmers [15].

To fully understand the interaction between the microswimmers, it is important to consider the near-field hydrodynamics. The pairwise interaction between two swimmers is not negligible even at large separations [16]. Experiments show that the cell-cell interaction between two swimming *Paramecia* is mainly governed by the hydrodynamic effects, rather than the biological interaction [2]. Two nearby *Volvox* colonies close to a solid surface are attracted toward each other and form stable bound states in which they dance around each other [1]. When in a suspension, the surface-mediated hydrodynamic interactions and the steric effects between the bacterial cells result in the formation of dynamic clusters and two-dimensional crystals [17,18]. Many theoretical and numerical works have been conducted to investigate the hydrodynamic interactions between two model swimmers in the Stokes regime. Based on the squirmer model, which comprises a spherical body with a tangential surface deformation to generate swimming motion, both analysis and simulations show that the two pullers will first attract each other, then they dramatically change their orientation during the near contact, and finally separate from each other [19]. Similar phenomena were also observed when including thermal fluctuations [20]. Two swimming bacteria, which use rotating helices to propel their cell bodies, considerably change their orientations and avoid each other [21]. When considering the details of the swimming stroke, the swimmer-swimmer interaction is complex depending on their relative displacement, orientation, and phase, leading to different scattering angles [22,23] and various types of motion, such as attraction, repulsion, or oscillation [24]. Another interesting phenomenon caused by the hydrodynamic interaction between two microswimmers is the enhancement of the swimming efficiency by synchronizing the phase of two adjacent flagella [25].

Previous studies of interacting microorganisms have been limited to the Stokes regime. The inertial effects are important for many planktonic swimmers in the transition regime [26],

*ardekani@purdue.edu

such as copepods, larvae, and *Pleurobrachia*. Inertial effects play an important role in changing the swimming direction of small organisms, attacking a prey, or escaping from a predator. For example, copepod *nauplii* exhibit unsteady motion during the escaping mode and the Reynolds number is about 6 [27]. In our previous studies, we have shown that the small but finite inertia causes a dramatic change to the near-wall motion of a swimmer [28] and the biogenic mixing efficiency [29]. One of the key differences due to the inertial effects is that the linearity of the governing equations in the Stokes regime breaks. Also, contrary to the zero Reynolds number regime, where the input power is fully dissipated into the surrounding fluid, in the inertial regime part of the power is used to accelerate the body.

In this article, we examine the hydrodynamic interaction of model swimmers in the small to intermediate Reynolds number regime, by means of direct numerical simulations. The inertial effects cause a significant change in the contact time and dispersion dynamics of swimmers. The results are helpful in better understanding the organisms' encounter dynamics and their collective behavior.

II. GOVERNING EQUATIONS AND NUMERICAL METHODS

The Navier-Stokes equations for an incompressible Newtonian fluid are solved in the entire computational domain

$$\rho\frac{D\boldsymbol{u}}{Dt} = -\nabla p + \nabla^2\boldsymbol{u} + \boldsymbol{f}, \tag{1a}$$

$$\nabla\cdot\boldsymbol{u} = \boldsymbol{0}, \tag{1b}$$

where $\boldsymbol{u}$ is the velocity, p is the pressure, and μ is the viscosity. The density ρ is equal to the swimmer density ρ_p inside the squirmer and equal to the fluid density ρ_f in the fluid domain. In this study, we set $\rho_p = \rho_f$ since the density of organisms is usually close to that of the background fluid. The swimmer is resolved by adding a forcing term inside the swimmer body using a distributed Lagrangian multiplier method [30], which is calculated by iteration as

$$\boldsymbol{f} = \boldsymbol{f}^* + \alpha\frac{\rho\phi}{\Delta t}(\boldsymbol{U} + \boldsymbol{\Omega}\times\boldsymbol{r} + \boldsymbol{u}_i - \boldsymbol{u}), \tag{2}$$

where $\boldsymbol{U}$ is the translational velocity of the squirmer, $\boldsymbol{\Omega}$ is the angular velocity, $\boldsymbol{u}_i$ is the imposed velocity causing the self-propulsion, $\boldsymbol{f}^*$ is the force calculated in the previous iteration, α is a dimensionless factor whose value affects the convergence rate but not the solution, and ϕ is the volume fraction occupied by the swimmer in each computational grid ($\phi = 1$ inside, $\phi = 0$ outside, and $0 < \phi < 1$ for the grids at the surface of the swimmer).

The squirmer model was introduced by Lighthill [31] and Blake [32] and has been historically used for swimmers (e.g. *Volvox*) in the Stokes regime. However, more recently the squirmer model has been extended to low and intermediate Reynolds number regimes [28,29,33–36]. This swimming model is the first step in understanding the effects of inertia and can predict the behavior of large ciliates, such as *Pleurobrachia*, in oceans and lakes. We consider the first two squirming modes. Consequently, the magnitude of the tangential velocity on the squirmer surface is written as

$$u_\theta^s(\theta) = B_1\sin\theta + B_2\sin\theta\cos\theta, \tag{3}$$

where θ is the polar angle measured from the swimming direction, and B_1 and B_2 are the first two squirming modes. The parameter $\beta = B_2/B_1$ distinguishes pullers ($\beta > 0$) and pushers ($\beta < 0$). In the Stokes regime, the swimming speed of a squirmer in an unbounded domain is $U_0 = 2B_1/3$. To recover the tangential velocity u_θ^s on the surface of the squirmer, we impose the following solenoidal velocity $\boldsymbol{u}_i$ inside the squirmer,

$$\boldsymbol{u}_i = \left[\left(\frac{r}{a}\right)^m - \left(\frac{r}{a}\right)^{m+1}\right]\left(u_\theta^s\cot\theta + \frac{du_\theta^s}{d\theta}\right)\boldsymbol{e}_r + \left[(m+3)\left(\frac{r}{a}\right)^{m+1} - (m+2)\left(\frac{r}{a}\right)^m\right]u_\theta^s\boldsymbol{e}_\theta, \tag{4}$$

where a is the radius of the squirmer, $\boldsymbol{e}_r$ and $\boldsymbol{e}_\theta$ are the unit vectors along the r and θ directions, and m is an arbitrary positive integer (the simulation results are independent of its value). The particle translational and angular velocities are calculated as

$$\boldsymbol{U} = \frac{1}{M_p}\int_{V_p}\rho_p(\boldsymbol{u} - \boldsymbol{u}_i)dV, \tag{5}$$

$$\mathbf{I}_p\boldsymbol{\Omega} = \int_{V_p}\rho_p\boldsymbol{r}\times(\boldsymbol{u} - \boldsymbol{u}_i)dV, \tag{6}$$

where V_p, M_p, and $\mathbf{I}_p$ are the volume, mass, and moment of inertia of the particle. Iterations are repeated until the maximum of Euclidean norm of $(\boldsymbol{f} - \boldsymbol{f}^*)/\boldsymbol{f}$ and the normalized residual fall below the specified tolerance of 10^{-3}.

When the squirmer approaches another squirmer, the high pressure in the thin film between the squirmers prevents any unphysical overlaps. However, a very small grid resolution is needed to resolve the thin liquid film and consequently it is computationally expensive. A repulsive force is imposed during the collision to prevent the unphysical overlap [37],

$$\boldsymbol{F}_r = \frac{C_m}{\varepsilon}\left(\frac{d - d_{\min} - dr}{dr}\right)^2\boldsymbol{e}, \tag{7}$$

where $C_m = M_pU_0^2/a$ is the characteristic force, $\varepsilon = 10^{-4}$ is a small positive number, d is the distance between two squirmers, $d_{\min} = 2a$ is the minimum possible distance, and dr is the force range and is set to be twice the smallest grid size Δ. The direction of the repulsive force $\boldsymbol{e}$ is along the squirmers line of centers.

Simulations are conducted using a finite volume method on a fixed staggered grid implemented in the code developed by Dabiri and co-workers [38–40]. A conventional operator splitting method is applied to enforce the continuity equation. The second-order total variation diminishing (TVD) Runge-Kutta method is used for time marching. The spatial derivatives in the convection term are evaluated using the quadratic upstream interpolation for convective kinetics (QUICK) scheme and the diffusion terms are discretized using the central difference scheme. The results are normalized by the characteristic length a, velocity $U_0 = 2B_1/3$, and time a/U_0. The mesh size and time step are $\Delta = 0.06$ and $\Delta t = 2.5\times10^{-4}$ for all the cases, except for $\mathrm{Re} = 0.1$, where we use $\Delta = 0.1$

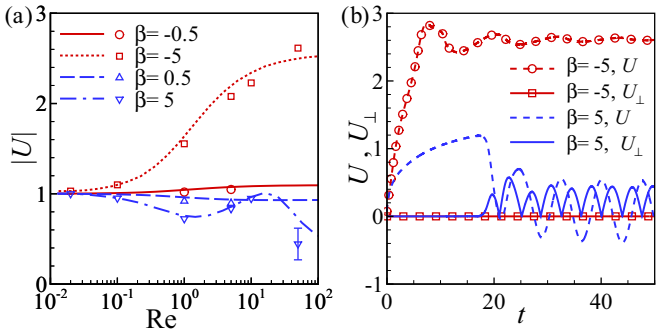

FIG. 1. (a) Swimming speed of a squirmer of $\beta = \pm 0.5$ and ± 5 at different Reynolds numbers. The symbols show the current results, and lines show previously published simulation results for a squirmer with a fixed orientation [36]. (b) Time history of the velocity components of a single squirmer of $\beta = \pm 5$ at $\mathrm{Re} = 50$. $U_\perp$ represents the velocity component perpendicular to the direction of the squirmer's orientation.

and $\Delta t = 10^{-3}$, and the diffusion terms are implicitly solved. Validation of the numerical method and the convergence studies are given in Secs. III A and III B. Additional validation and verification tests using this code can be found in our previous publications [28,29,41,42].

III. RESULTS

A. Swimming motion of a single squirmer

The motion of a single squirmer in an unbounded fluid is first investigated. Figure 1(a) shows the magnitude of the swimming speed at various Reynolds numbers. A pusher swims faster while a puller swims slower with increasing Re. From the perturbation theory [34], the swimming speed of a squirmer in an unbounded domain is $U \approx 1\text{–}0.15\beta\,\mathrm{Re}$ and holds well for $\mathrm{Re} < 0.1$ [28]. Our results agree with the previous simulations [36] for pushers and for pullers at $\mathrm{Re} < 10$. At higher Re, the puller becomes unstable and the previous results of a squirmer with a fixed orientation [36] does not describe the behavior of a freely swimming squirmer. The swimming motion of a pusher is always stable in the range of Reynolds number investigated in this article. The velocity field away from the squirmer in the swimming direction decays approximately as $|u| \sim r^{-3}$ when swimming in a finite

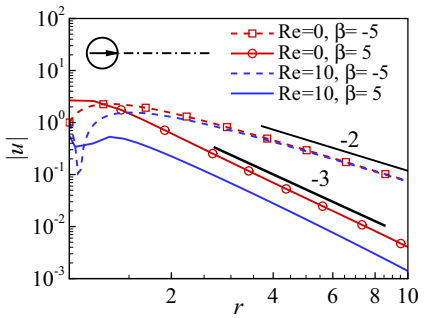

FIG. 2. Velocity magnitude away from an isolated squirmer in the swimming direction for $\mathrm{Re} = 0$ and 10.

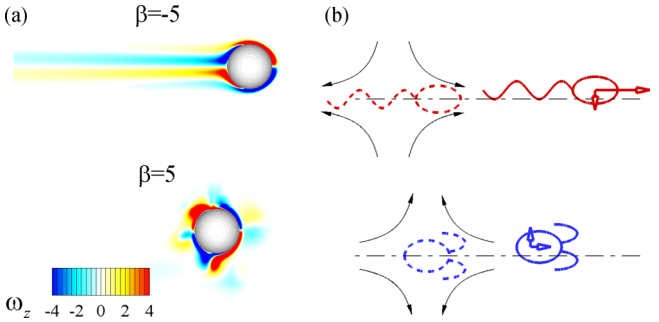

FIG. 3. (a) Vorticity field ω_z around a single pusher of $\beta = -5$ (top) and puller of $\beta = 5$ (bottom) at $\mathrm{Re} = 50$. (b) Schematic representation of inertial effects on the swimming motion of a single pusher and puller.

Reynolds number regime. On the other hand, far field velocity of a Stokes squirmer behaves as a force dipole $|u| \sim r^{-2}$ (see Fig. 2). The velocity decay of swimming zooplankton, such as *Mesodinium rubrum* and *Podon intermedius*, is closer to an inertial squirmer than a Stokes squirmer [43].

Figure 1(b) shows the time history of a single squirmer of $\beta = \pm 5$ at $\mathrm{Re} = 50$. For a pusher, the initial oscillation in the speed eventually dampens out and it will swim with a constant speed. A pusher has a long vorticity wake, as shown in Fig. 3(a). In contrast, the swimming motion of a puller becomes unstable at $\mathrm{Re} \sim O(10)$, leading to a three-dimensional swimming trajectory. The vorticity field is also more complex for an unstable puller. These observations can be explained by the following arguments. With increasing Re, the history effects become important and the swimmer is more affected by the flow field induced by itself at a previous time [see Fig. 3(b)]. The pusher is "pushed" to swim faster due to the velocity field induced by itself at an earlier time (dashed swimmer), while the puller is "pulled" and swims slower. The stability of the swimmer is also related to the hydrodynamic interaction between its body and the velocity field created by its movement. A pusher will return to its original trajectory due to the hydrodynamic attraction if it is laterally perturbed away from the straight trajectory. The response of a puller is exactly opposite, and its trajectory becomes unstable with increasing inertial effect.

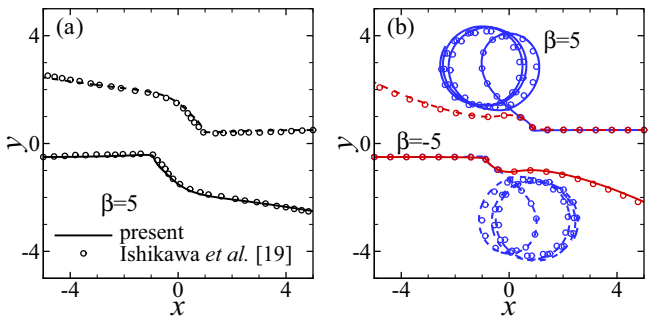

FIG. 4. (a) Comparison of the trajectories of two colliding pullers. Present results correspond to $\mathrm{Re} = 0.1$ and previous results are obtained for Stokes flow [19]. (b) Comparison of the trajectories of two squirmers at $\mathrm{Re} = 10$ using different grid resolutions, $\Delta = 0.06$ (line) and 0.04 (symbols).

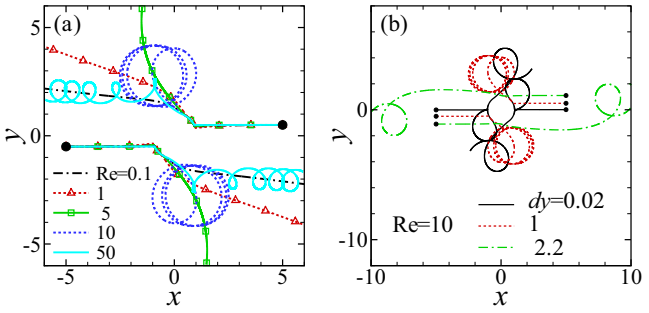

FIG. 5. (a) Trajectories of two pullers of $\beta = 5$ at different Reynolds numbers. (b) Trajectories of two pullers at Re = 10 and different dy.

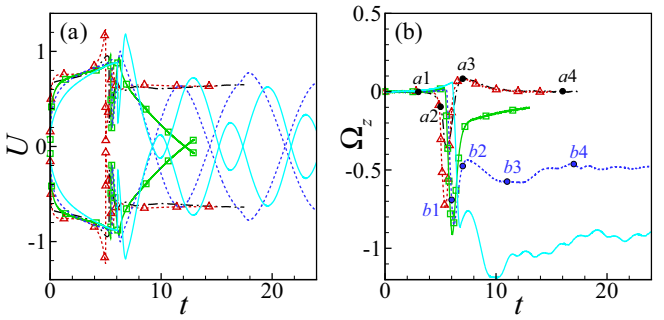

FIG. 7. Time history of (a) U-velocity component and (b) angular velocity Ω_z of two pullers of $\beta = 5$ at different Reynolds numbers. Legends are the same as Fig. 5(a).

B. Pairwise interaction of two pullers

In this section, we consider the pairwise interactions of two pushers ($\beta = -5$) and two pullers ($\beta = 5$) which are initially located in the same plane ($z = 0$). They initially swim towards each other and their swimming orientations are initially parallel. The distance between their centers is dx and dy in the x and y directions, respectively. We set $dx = 10$ and $dy = 1$ unless otherwise mentioned. As shown in Fig. 4(a), our results of two pullers at Re = 0.1 agree well with previously published results [19] in the Stokes regime. Further, convergence studies performed for squirmers at a higher Reynolds number (Re = 10) show that the results are independent of mesh size [see Fig. 4(b)].

The hydrodynamic interaction of two pullers is dramatically modified by the presence of inertia. To illustrate this, the comparison of the trajectories of two pullers at different Reynolds numbers is shown in Fig. 5(a). Figure 6 shows the time evolution of the flow field and the pullers' swimming trajectories at different Reynolds numbers. At Re = 0.1 and 1, the two pullers rotate away from each other during the collision and eventually escape with positive scattering angles. The recirculating regions with a high vorticity value ω_z in front of and behind an isolated swimmer at Re = 0.1 have a similar shape and size [see Fig. 6(a1)]. At higher Reynolds numbers, the pullers generate larger recirculating regions behind their body, which are similar to the ones observed for a cruising

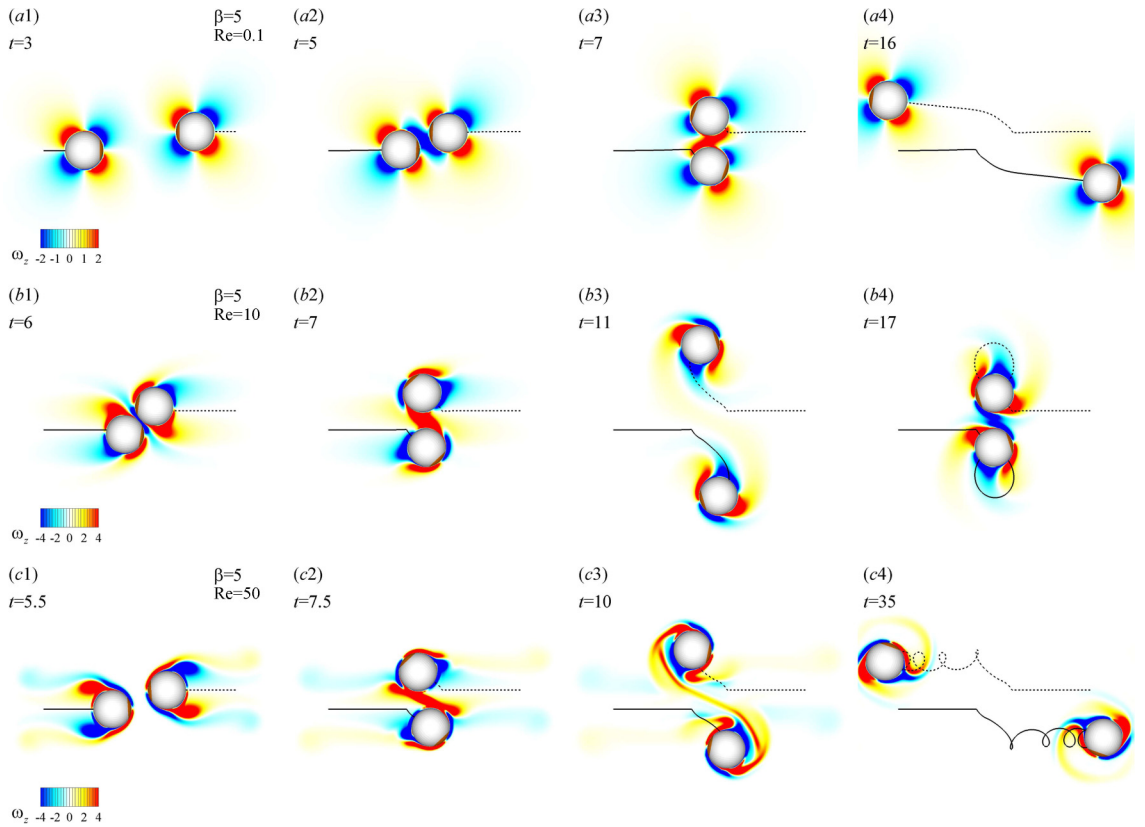

FIG. 6. Time sequence of the swimming motion of two pullers of $\beta = 5$ at (a1)–(a4) Re = 0.1, (b1)–(b4) Re = 10, and (c1)–(c4) Re = 50. The contour plots show the vorticity ω_z in the plane $z = 0$. The black lines show the trajectories of the swimmers. For movies, see Ref. [46].

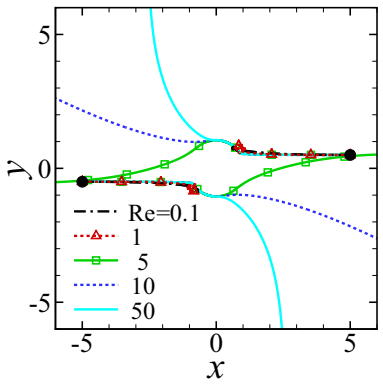

FIG. 8. Trajectories of two pushers of $\beta = -5$ at different Reynolds numbers.

Metridia longa [43]. The rotation of the swimmer is so strong that the trajectories become circular after the separation. The vorticity field is strongly disturbed due to the spinning motion of the pullers [see Figs. 6(b1)–6(b4) and 6(c1)–6(c4)]. Notably, the two pullers at $\mathrm{Re} = 10$ are hydrodynamically entrapped near each other as they are rotating in circular trajectories for a long time. At $\mathrm{Re} = 50$, the two pullers swim away from each other following circular trajectories with small radii of curvature. The trajectories of two pullers at $\mathrm{Re} = 10$ under different initial configurations $dy = 0.02$ and $dy = 2.2$ are plotted in Fig. 5(b). It is clear that the details of trajectories are closely related to the initial condition, but the hydrodynamic entrapment in circular trajectories exists for different Reynolds numbers above $\mathrm{Re} \sim 10$ and different initial lateral distances. These observations are qualitatively similar to the bound states of two dancing spherical alga *Volvox* near a surface [1]. However, the mechanisms in the two cases are very different. The corresponding Reynolds number of a *Volvox* is around 0.03, and the formation of a bound state occurs due to the *Volvox* swimming motion near a boundary. Here, the inertial effects lead to the instability of the swimming motion of a single puller, as discussed in Sec. III A, which dramatically modifies the hydrodynamic interaction between the two swimmers.

Figure 7 shows the time evolution of the U-velocity component and the angular velocity Ω_z of the pullers at different Reynolds numbers. The U velocity of the pullers quickly drops during the collision and then it recovers and reaches a peak value. After they separate from each other, the puller at low Re swims with a roughly constant speed, which is reduced compared to the swimming speed of a single squirmer due to the flow field induced by the other squirmer. At higher Re, the U velocity oscillates. The pullers always rotate in a clockwise direction during the collision, as shown in Fig. 7(b). The vorticity in the gap region between the two swimmers is first negative as the swimmers get close to each other [see Fig. 6(a2)]. Then the magnitude of Ω_z decreases after the two swimmers pass each other [see Fig. 6(a4)]. At low Re, the angular velocity becomes positive due to the strong induced

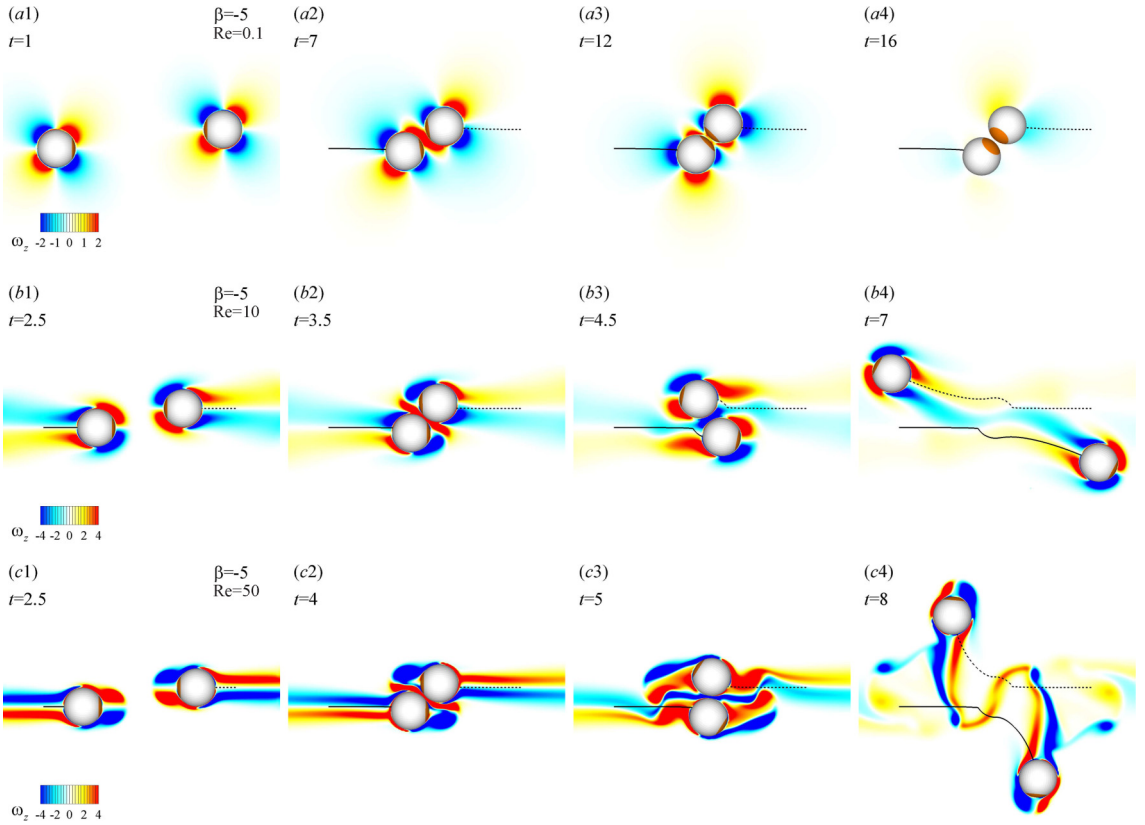

FIG. 9. Time sequence of the swimming motion of two pushers of $\beta = -5$ at (a1)–(a4) $\mathrm{Re} = 0.1$, (b1)–(b4) $\mathrm{Re} = 10$, and (c1)–(c4) $\mathrm{Re} = 50$. The contour plots show the vorticity ω_z in the plane $z = 0$. The black lines show the trajectories of the swimmers. For movies, see Ref. [46].

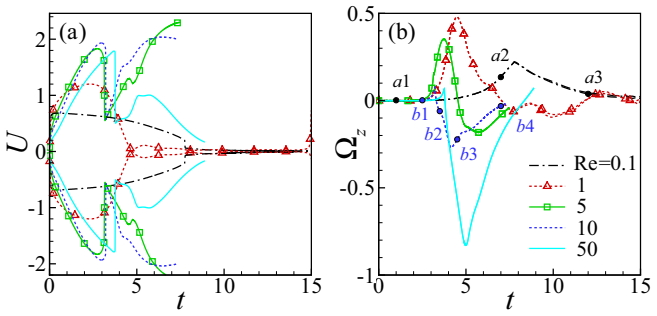

FIG. 10. Time history of (a) U-velocity component and (b) angular velocity Ω_z of two pushers of $\beta = -5$ at different Reynolds numbers.

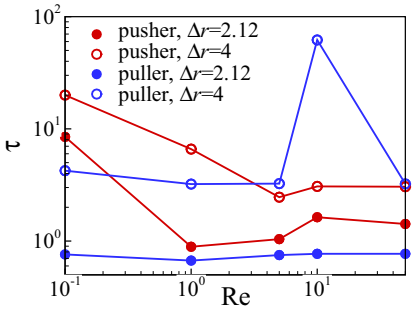

FIG. 11. Contact ($\Delta r \leqslant 2.12$) and nearby ($\Delta r \leqslant 4$) time τ of two squirmers of $\beta = \pm 5$ at different Reynolds numbers.

rotating effects from the vorticity field, and it then gradually goes to zero as the two swimmers separate from each other. At high Re, the inertial effects greatly enhance the initial rotation in the clockwise direction, and the pullers maintain a high angular velocity after their separation and swim in circular trajectories.

C. Pairwise interaction of two pushers

In Fig. 8, we compare the trajectories of two pushers of $\beta = -5$ at different Reynolds numbers. Their flow fields are shown in Fig. 9. At Re = 0.1, the two pushers stay in close contact for a long time after the collision. Meanwhile, they rotate towards each other and get trapped. This state is unstable, and the two pushers eventually swim away and leave their initial swimming plane. At higher Reynolds numbers, the squirmers keep swimming in their initial plane after collision, and the scattering angle strongly depends on the Reynolds number. At Re = 5, the scattering angle is negative, while at Re = 50, the scattering angle is almost positive 90°. A long vorticity wake is formed behind the pushers at Re = 10 and 50, as shown in Fig. 9, where its magnitude is stronger than the wake vorticity at Re = 0.1. After the two pushers pass each other, their vorticity wakes have strong effects on their motion, causing them to rotate in a clockwise direction. The interaction between the two wakes is stronger at higher Re. As seen in Fig. 9(c4), the elongated wakes become unstable and generate ringlike vortical structures in three dimensions.

The U velocity and the angular velocity Ω_z of the pushers are shown in Fig. 10. At Re = 0.1, the swimming speed of the pushers gradually decreases as they approach each other. As the swimmers get close, they lose their momentum and are not able to pass each other. Meanwhile, the swimmers keep rotating in a counterclockwise direction before their heads-on collision. They spend a long time in the heads-on configuration until eventually small perturbations lead to their reorientation and they eventually escape. At higher Reynolds numbers (Re = 10,50), the pushers swim much faster and their angular velocity only slightly increases before they collide. The swimmers at higher Reynolds numbers maintain a high momentum before collision and they easily pass each other. The inertial effects also cause the swimmers to rotate in a clockwise direction [Fig. 9(b2)] as opposed to counterclockwise rotation in the low Reynolds number regime [Fig. 9(a2)]. Eventually, the two swimmers escape from each other, staying in their initial plane.

D. Contact time of two swimmers

In Fig. 11, we quantify the inertial effects on the contact time τ of the two squirmers. The contact time is defined as the time duration when the distance between the center of the squirmers is smaller than $\Delta r = 2.12$, where the repulsive collision force is nonzero. The collision time is greatly reduced for pushers at higher Re, while it is less affected for pullers. We also define the nearby time which is the time duration when the distance between the center of squirmers is smaller than twice their diameter. For the pushers, the same trend is observed for the nearby time as the contact time. For the pullers, nearby time is affected due to the entrapment of the pullers in a circular loop. The two pullers at Re = 10 stay around each other for a much longer time. These results are important in estimating the encounter time for organisms, which is essential in reproduction, feeding, and escaping from a predator. For example, experiments show that the male calanoid copepod species *T. longicornis* locate and pursue females within twice the body length from a female's swimming path, following odor tracers [44]. They accelerate and the Reynolds number changes from 5–15 typical of a normal swimming mode to 11–40 during pursuit [45]. In this example, both their hydrodynamic interaction and the distribution of the odor tracers are greatly affected by the inertial effects.

IV. CONCLUSIONS

In this study, we numerically investigated the effects of inertia on the swimming motion and the pairwise hydrodynamic interactions of small organisms. The squirmer model is used, representing two types of swimming strategies typically encountered in motile cells: pullers and pushers. With increasing Re, a squirmer interacts with the flow field induced by itself at an earlier time. As a result, a pusher swims faster in a straight line, while a puller swims slower and its swimming trajectory is unstable. The contact time of two interacting pushers is reduced by increasing inertial effects. In contrast, a pair of pullers at Re $\sim$ 10 move in circular trajectories and stay near each other for a long time. The pairwise interaction of organisms is the first critical step to gain a fundamental understanding of the collective behavior of

small organisms. Our results show that the inertial effects can greatly affect the biophysical interactions of small organisms. In this work, we focus on the role of inertial effects on a simplified swimmer model to have a tractable number of parameters in the problem. But in nature, the swimming motion of many organisms is highly unsteady. Previous studies have used a squirmer model with an unsteady slip velocity [33,47], which involves more parameters in the physical space. The details of the unsteadiness and the swimming kinematics could have important effects on the hydrodynamic interaction of inertial swimmers. Further studies are required to include these effects.

ACKNOWLEDGMENTS

This publication was made possible, in part, with support from NSF (CBET-1445955-CAREER and CBET-1604423). A.O. acknowledges the Martin and Carmel Naughton Graduate Fellowship.

[1] K. Drescher, K. C. Leptos, I. Tuval, T. Ishikawa, T. J. Pedley, and R. E. Goldstein, Dancing Volvox: Hydrodynamic Bound States of Swimming Algae, Phys. Rev. Lett. **102**, 168101 (2009).

[2] T. Ishikawa and M. Hota, Interaction of two swimming paramecia, J. Exp. Biol. **209**, 4452 (2006).

[3] T. Kiørboe, H. Jiang, and S. P. Colin, Danger of zooplankton feeding: The fluid signal generated by ambush-feeding copepods, Proc. R. Soc. London, Ser. B **277**, 3229 (2010).

[4] C. Dombrowski, L. Cisneros, S. Chatkaew, R. E. Goldstein, and J. O. Kessler, Self-Concentration and Large-Scale Coherence in Bacterial Dynamics, Phys. Rev. Lett. **93**, 098103 (2004).

[5] A. Sokolov, I. S. Aranson, J. O. Kessler, and R. E. Goldstein, Concentration Dependence of the Collective Dynamics of Swimming Bacteria, Phys. Rev. Lett. **98**, 158102 (2007).

[6] X. Wu and A. Libchaber, Particle Diffusion in a Quasi-Two-Dimensional Bacterial Bath, Phys. Rev. Lett. **84**, 3017 (2000).

[7] Y. Sumino, K. H. Nagai, Y. Shitaka, D. Tanaka, K. Yoshikawa, H. Chaté, and K. Oiwa, Large-scale vortex lattice emerging from collectively moving microtubules, Nature (London) **483**, 448 (2012).

[8] I. Riedel, K. Kruse, and J. Howard, A self-organized vortex array of hydrodynamically entrained sperm cells, Science **309**, 300 (2005).

[9] J. R. Howse, R. A. Jones, A. J. Ryan, T. Gough, R. Vafabakhsh, and R. Golestanian, Self-Motile Colloidal Particles: From Directed Propulsion to Random Walk, Phys. Rev. Lett. **99**, 048102 (2007).

[10] V. Narayan, S. Ramaswamy, and N. Menon, Long-lived giant number fluctuations in a swarming granular nematic, Science **317**, 105 (2007).

[11] J. K. Parrish and L. Edelstein-Keshet, Complexity, pattern, and evolutionary trade-offs in animal aggregation, Science **284**, 99 (1999).

[12] F. E. Fish, Kinematics of ducklings swimming in formation: Consequences of position, J. Exp. Zool. **273**, 1 (1995).

[13] A. D. Becker, H. Masoud, J. W. Newbolt, M. Shelley, and L. Ristroph, Hydrodynamic schooling of flapping swimmers, Nat. Commun. **6**, 8514 (2015).

[14] A. T. Chwang and T. Y. Wu, Hydromechanics of low-Reynolds-number flow. Part 2. Singularity method for Stokes flows, J. Fluid Mech. **67**, 787 (1975).

[15] E. Lauga and T. R. Powers, The hydrodynamics of swimming microorganisms, Rep. Prog. Phys. **72**, 096601 (2009).

[16] R. J. Clarke, M. D. Finn, and M. MacDonald, Hydrodynamic persistence within very dilute two-dimensional suspensions of squirmers, Proc. R. Soc. London, Ser. A **470**, 20130508 (2014).

[17] X. Chen, X. Yang, M. Yang, and H. P. Zhang, Dynamic clustering in suspension of motile bacteria, Europhys. Lett. **111**, 54002 (2015).

[18] A. P. Petroff, X.-L. Wu, and A. Libchaber, Fast-Moving Bacteria Self-Organize into Active Two-Dimensional Crystals of Rotating Cells, Phys. Rev. Lett. **114**, 158102 (2015).

[19] T. Ishikawa, M. P. Simmonds, and T. J. Pedley, Hydrodynamic interaction of two swimming model micro-organisms, J. Fluid Mech. **568**, 119 (2006).

[20] I. O. Götze and G. Gompper, Mesoscale simulations of hydrodynamic squirmer interactions, Phys. Rev. E **82**, 041921 (2010).

[21] T. Ishikawa, G. Sekiya, Y. Imai, and T. Yamaguchi, Hydrodynamic interactions between two swimming bacteria, Biophys. J. **93**, 2217 (2007).

[22] G. P. Alexander, C. M. Pooley, and J. M. Yeomans, Scattering of low-Reynolds-number swimmers, Phys. Rev. E **78**, 045302 (2008).

[23] A. Furukawa, D. Marenduzzo, and M. E. Cates, Activity-induced clustering in model dumbbell swimmers: The role of hydrodynamic interactions, Phys. Rev. E **90**, 022303 (2014).

[24] C. M. Pooley, G. P. Alexander, and J. M. Yeomans, Hydrodynamic Interaction Between Two Swimmers at Low Reynolds Number, Phys. Rev. Lett. **99**, 228103 (2007).

[25] G. J. Elfring and E. Lauga, Hydrodynamic Phase Locking of Swimming Microorganisms, Phys. Rev. Lett. **103**, 088101 (2009).

[26] J. Yen, Life in transition: Balancing inertial and viscous forces by planktonic copepods, Biol. Bull. **198**, 213 (2000).

[27] B. J. Gemmell, J. Sheng, and E. J. Buskey, Compensatory escape mechanism at low Reynolds number, Proc. Natl. Acad. Sci. USA **110**, 4661 (2013).

[28] G.-J. Li and A. M. Ardekani, Hydrodynamic interaction of microswimmers near a wall, Phys. Rev. E **90**, 013010 (2014).

[29] S. Wang and A. M. Ardekani, Biogenic mixing induced by intermediate Reynolds number swimming in stratified fluids, Sci. Rep. **5**, 17448 (2015).

[30] A. M. Ardekani, S. Dabiri, and R. Rangel, Collision of multi-particle and general shape objects in a viscous fluid, J. Comput. Phys. **227**, 10094 (2008).

[31] M. J. Lighthill, On the squirming motion of nearly spherical deformable bodies through liquids at very small Reynolds numbers, Commun. Pure Appl. Math. **5**, 109 (1952).

[32] J. R. Blake, A spherical envelope approach to ciliary propulsion, J. Fluid Mech. **46**, 199 (1971).

[33] S. Wang and A. M. Ardekani, Unsteady swimming of small organisms, J. Fluid Mech. **702**, 286 (2012).

[34] S. Wang and A. Ardekani, Inertial squirmer, Phys. Fluids **24**, 101902 (2012).
[35] A. Doostmohammadi, R. Stocker, and A. M. Ardekani, Low-Reynolds-number swimming at pycnoclines, Proc. Natl. Acad. Sci. USA **109**, 3856 (2012).
[36] N. G. Chisholm, D. Legendre, E. Lauga, and A. S. Khair, A squirmer across Reynolds numbers, J. Fluid Mech. **796**, 233 (2016).
[37] R. Glowinski, T. W. Pan, T. I. Hesla, D. D. Joseph, and J. Periaux, A fictitious domain approach to the direct numerical simulation of incompressible viscous flow past moving rigid bodies: Application to particulate flow, J. Comput. Phys. **169**, 363 (2001).
[38] S. Dabiri, J. Lu, and G. Tryggvason, Transition between regimes of a vertical channel bubbly upflow due to bubble deformability, Phys. Fluids **25**, 102110 (2013).
[39] S. Dabiri and G. Tryggvason, Heat transfer in turbulent bubbly flow in vertical channels, Chem. Eng. Sci. **122**, 106 (2015).
[40] S. Dabiri, A. Doostmohammadi, M. Bayareh, and A. M. Ardekani, Rising motion of a swarm of drops in a linearly stratified fluid, Int. J. Multiphase Flow **69**, 8 (2015).
[41] G.-J. Li, A. Karimi, and A. M. Ardekani, Effect of solid boundaries on swimming dynamics of microorganisms in a viscoelastic fluid, Rheol. Acta **53**, 911 (2014).
[42] G. Li, G. H. McKinley, and A. M. Ardekani, Dynamics of particle migration in channel flow of viscoelastic fluids, J. Fluid Mech. **785**, 486 (2015).
[43] T. Kiørboe, H. Jiang, R. J. Gonçalves, L. T. Nielsen, and N. Wadhwa, Flow disturbances generated by feeding and swimming zooplankton, Proc. Natl. Acad. Sci. USA **111**, 11738 (2014).
[44] M. J. Weissburg, M. H. Doall, and J. Yen, Following the invisible trail: Kinematic analysis of mate-tracking in the copepod temora longicornis, Philos. Trans. R. Soc. B **353**, 701 (1998).
[45] M. H. Doall, S. P. Colin, J. R. Strickler, and J. Yen, Locating a mate in 3D: The case of temora longicornis, Philos. Trans. R. Soc. B **353**, 681 (1998).
[46] See Supplemental Material at http://link.aps.org/supplemental/10.1103/PhysRevE.94.053104 for the videos of two interacting pushers and pullers.
[47] V. Magar and T. J. Pedley, Average nutrient uptake by a self-propelled unsteady squirmer, J. Fluid Mech. **539**, 93 (2005).